Special Feature: Innovative Technologies for the Automotive Structure and Processing

Research Report

Virtual Material Testing Based on Computational Homogenization Using Statistically Similar Representative Volume Elements for Short Fiber Composites

Takashi Sasagawa, Masato Tanaka and Ryuji Omote

■**ABSTRACT**‖ A computational method is presented for the construction of statistically similar representative volume elements (SSRVEs) for short fiber composites (SFCs) to realize efficient calculation of their mechanical properties based on computational homogenization. The SSRVEs are obtained as a solution of an optimization problem that minimizes the difference between the power spectral density of a target microstructure and that of a SSRVE. The proposed method is applied to a virtually generated target microstructure that serves as an example for a SFC and is validated by comparison of the mechanical properties of the target microstructure with those of the SSRVE. The results demonstrate that the mechanical properties of the SSRVE are consistent with those of the target microstructure and that the SSRVEs can significantly reduce the computational costs of finite element analyses used to derive the macroscopic mechanical properties of SFCs.

1. Introduction

Short fiber composites (SFCs) that use thermoplastics[1] are spotlighted as an advanced material for lightweight structures. It is essential to evaluate the mechanical properties to ensure the safety of lightweight products made of SFCs. A series of material tests is one of the options for achieving this. An alternative way is to use analytical calculations based on mean field methods such as Eshelby's inclusion,[2] the Mori-Tanaka theory[3] or the self-consistent model.[4] Nonlinear mechanical behavior may be predicted using incremental Eshelby-Mori-Tanaka approach procedures,[5] where the nonlinearity of a matrix is linearized with each increment and the nonlinear behavior of the composites is calculated based on the Mori-Tanaka theory with the linearized properties. Fiber orientation distributions may also be considered using orientation tensors[6] within the analytical estimation methods.[5]

Numerical material testing[7-9] (NMT) based on computational homogenization methods[10-14] is also a powerful tool as an alternative method to predict the mechanical properties of composites made of nonlinear materials. In NMT, stress-strain relationships can be obtained based on the volume averages of microscopic stress and strain. The microscopic stress and strain are computed by solving boundary value problems using representative volume elements (RVEs). NMT can be used to estimate macroscopic characteristics with consideration of the volume fraction, the geometric dimensions, and the direction distribution of the fibers in the RVEs. One shortcoming of NMT is its high computational cost. NMT of SFCs could be especially expensive because classical RVEs of SFCs are complex due to the aspect ratio of carbon fibers. For example, an RVE constructed using computed tomography (CT) data of SFCs consists of approximately 10 million elements.[15]

Balzani et al. proposed a computational method of statistically similar RVEs (SSRVEs).[16] SSRVEs are simplified microstructures that sufficiently reflect the morphology of real microstructures in terms of statistical measures. Therefore, the computational cost of NMT can be significantly reduced because the simplified morphology leads to a more efficient numerical discretization. The reliability of the SSRVEs

for dual-phase steels was validated in the literature.[17-20] However, the original computational methodology using SSRVEs for dual-phase steel may not be applied directly to SFCs, because the microstructure of SFCs is quite different from that of dual-phase steels.

This article provides an extended construction method of SSRVEs for SFCs. The outline of the article is as follows. In Sec. 2, an optimization scheme is proposed to construct SSRVEs for SFCs. Section 3 provides verification results of the optimization scheme through a simple 3D example with a trivial solution. In Sec. 4, SSRVEs for SFCs are constructed using a real target microstructure and the proposed method is validated by comparison of the mechanical properties of the target microstructures with those of the SSRVEs. Conclusions are given in Sec. 5.

2. Construction Method of SSRVEs for SFCs

SSRVEs are simplified microstructures, of which the statistics are similar to those of the given target microstructures. For SSRVEs of a dual-phase steel, the power spectral density (PSD), the lineal-path function and the Minkowski functionals were applied as statistical descriptors.[16,21,22] The PSD computed from microstructures leads to information regarding the periodicity of the size, shape, orientation and distance of inclusions. The lineal-path function and Minkowski functionals capture the size and shape distribution of inclusions. In the proposed method, the size and shape distribution of inclusions are already given by modeling fibers in the SSRVEs with cylinders having a prescribed length and diameter. The angle and position of each fiber are also computed based on the PSD. The optimal parameterization $\tilde{\gamma}$, of the SSRVE is then obtained by the following the optimization problem:

$$\tilde{\gamma} = \arg\left\{ \min_{\gamma}\left[\mathcal{E}\left(\gamma\right)\right]\right\}, \tag{1}$$

where $\mathcal{E}$ is the objective function and γ is the design variable that describes the microstructure morphology of the SSRVE, which is defined as:

$$\gamma = \left[\gamma_1^T, \gamma_2^T, \cdots, \gamma_i^T, \cdots, \gamma_{N_{fiber}}^T\right]^T. \tag{2}$$

Herein, γ_i is the design parameter vector with respect to the i-th fiber of N_{fiber} fibers in the SSRVE. The shape of the fibers is assumed to be cylindrical in the present

model. The fiber orientation angles (φ, θ) depicted in **Fig. 1** and the center coordinates (c_x, c_y, c_z) of the fibers are stored in γ such that:

$$\gamma_i = \begin{cases} \left\{\varphi_i, \theta_i\right\}^T, & \text{if } i = 1, \\ \left\{c_{x,i}, c_{y,i}, c_{z,i}, \varphi_i, \theta_i\right\}^T, & \text{otherwise.} \end{cases} \tag{3}$$

Here, note that the fiber center coordinates are not stored in γ_1, because the position of the first fiber is fixed at the center of the SSRVE to exclude a simple translation of the inclusion phase, which would enable an infinite number of equal solutions to the optimization problem in Eq. (1). In this work, the number, length, and diameter of the fibers, and the size of the SSRVE were assumed to be constants that were reasonably defined based on measurements of the real microstructure.

In the optimization problem of Eq. (1), the objective function $\mathcal{E}$ is defined as:

$$\mathcal{E}\left(\gamma\right) = \frac{1}{\hat{N}_x \hat{N}_y \hat{N}_z} \sum_{j=1}^{\hat{N}_x} \sum_{k=1}^{\hat{N}_y} \sum_{l=1}^{\hat{N}_z} \\ \left[\mathcal{S}_{jkl}\left(\chi^{\text{target}}, R_x^{\text{target}}, R_y^{\text{target}}, R_z^{\text{target}}\right) \\ - \mathcal{S}_{jkl}\left(\chi^{\text{SSRVE}}\left(\gamma\right), R_x^{\text{SSRVE}}, R_y^{\text{SSRVE}}, R_z^{\text{SSRVE}}\right)\right]^2, \tag{4}$$

where $\mathcal{S}_{jkl}$ is the rebinned PSD of the microstructure computed for a discrete set of $\hat{N}_x \times \hat{N}_y \times \hat{N}_z$ voxels,
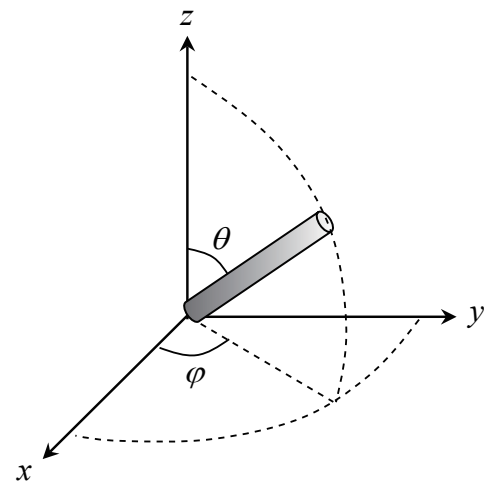
Fig. 1 Definition of angles describing the longitudinal direction of a fiber.

the subscripts "*x*", "*y*" and "*z*" indicate components for the *x*-, *y*- and *z*-directions, and the superscripts "target" and "SSRVE" indicate quantities of the target microstructure and the SSRVE, respectively.

The voxel data χ, which describes the binarized microstructure, is defined as:

$$\chi_{pqr}^{A} = \begin{cases} 1, & \text{if } \boldsymbol{x}_{pqr}^{A}\left(n_x^A, n_y^A, n_z^A\right) \in D^A, \\ 0, & \text{otherwise,} \end{cases}$$

with $p = 1, \cdots, N_x^A$, $q = 1, \cdots, N_y^A$, $r = 1, \cdots, N_z^A$,   (5)

where $\boldsymbol{x}$ is the center coordinate vector of each voxel for χ, and D is the domain of each fiber. The superscript "A" represents either the target or SSRVE. In addition, N_x, N_y, and N_z indicate the size of χ, and the subscripts p, q, and r denote the indices of the corresponding voxels in the *x*, *y*, and *z* directions, respectively. Note that only D^{SSRVE} is a function of the design variable γ.

The rebinned PSD, $\mathcal{S}_{jkl}$ in Eq. (4), is given by:

$$\mathcal{S}_{jkl}\left(\chi^A, R_x^A, R_y^A, R_z^A\right) = \frac{s_{jkl}\left(\chi^A, R_x^A, R_y^A, R_z^A\right)}{s_{\max}\left(\chi^A, R_x^A, R_y^A, R_z^A\right)},   (6)$$

$$s_{jkl}\left(\chi^A, R_x^A, R_y^A, R_z^A\right)$$
$$= \frac{1}{R_x^A R_y^A R_z^A}\sum_{t=R_x^A(j-1)+1}^{jR_x^A}\sum_{u=R_y^A(k-1)+1}^{kR_y^A}\sum_{v=R_z^A(l-1)+1}^{lR_z^A}\mathcal{P}_{tuv}\left(\chi^A\right),$$
(7)

where $s_{\max}$ is the maximum component value of $\boldsymbol{s}$, and R_x, R_y, and R_z, which describe the ratios between $\hat{N}$ and N, are defined as:

$$R_x^A = \frac{N_x^A}{\hat{N}_x}, \qquad R_y^A = \frac{N_y^A}{\hat{N}_y}, \qquad R_z^A = \frac{N_z^A}{\hat{N}_z}.   (8)$$

Moreover, $\mathcal{P}_{tuv}$ in Eq. (7) is the PSD of the microstructure defined as:

$$\mathcal{P}_{tuv}\left(\chi^A\right) = \left|\mathcal{F}_{tuv}\left(\chi^A\right)\right|^2 = \mathcal{F}_{tuv}^{*}\left(\chi^A\right)\mathcal{F}_{tuv}\left(\chi^A\right),   (9)$$

where $\mathcal{F}_{tuv}$ is the $N_x \times N_y \times N_z$ voxel data obtained from the Fourier transform of χ, and $\mathcal{F}_{tuv}^{*}$ is the conjugate complex of $\mathcal{F}_{tuv}$.

The total number N^{target} of voxels of χ^{target} cannot be coincident with the total number N^{SSRVE} of voxels of χ^{SSRVE}. This will automatically be the case when the number of voxels in the physical space, i.e., of the microstructure morphology itself, differs because the target microstructure is larger than the SSRVE. This can easily be avoided by rebinning the PSD of the SSRVE and the target microstructure, as shown in Eqs. (7) and (8). Note that the trivial entry $\mathcal{P}_{111}$ is removed before the calculation of the rebinned PSD $\mathcal{S}_{jkl}$, because it provides no information and is just redundant.

The objective function $\mathcal{E}$ in Eq. (1) is discrete, i.e., non-differentiable and generally non-convex.[16] Therefore, the global optimization toolbox in MATLAB (R2016b), which is based on genetic algorithms, is used. The fast Fourier transform in MATLAB is also used for the computation of $\mathcal{F}_{tuv}$ in Eq. (9). In this scheme, a global minimum may not be guaranteed due to the non-convexity of the objective function, $\mathcal{E}$. However, the obtained minimum will be mechanically analyzed in the sense that the mechanical response of the SSRVE is similar to that of the target microstructure. In this case, the SSRVE is considered appropriate.

3. Verification with Simple Examples

In this section, the influence of the microstructure morphology on the PSD is first shown using 2D examples. The optimization scheme proposed in the previous section is then verified through a simple 3D example.

3. 1 2D Examples of PSD

The influence of three types of microstructure morphology on their respective PSDs is summarized in **Fig. 2**. Three series of microstructures and their PSD are respectively shown on the left and right sides of Figs. 2(a)-(c). The white and black phases in the microstructures describe the domains that satisfy $\chi_{pqr}^{A} = 1$ and $\chi_{pqr}^{A} = 0$, respectively; therefore, the white phase describes the fibers in this example. The PSD describes the normalized $\mathcal{P}_{tuv}$ and the origin of $\mathcal{P}_{tuv}$ is located at the center of the PSD. Figure 2(a) shows that the distribution of the PSD is related to the rotation of the fiber. The distribution of the PSD becomes narrower as the fiber length becomes longer, as shown in Fig. 2(b). Finally, Fig. 2(c) shows that the peak interval of the PSD distribution becomes smaller as the interval of fibers becomes larger. These results show that the PSD of a microstructure is strongly correlated with the

fiber orientation, fiber length and fiber distance. The SSRVEs are then constructed based on the PSD of the target microstructures according to these results.

3. 2 Verification of Optimization Scheme

The proposed optimization procedure is verified through a simple 3D example that already has a known solution. The target microstructure consists of two fibers embedded in a matrix, and the SSRVE also consists of two fibers and a matrix, as shown in **Fig. 3**. The initial SSRVE shown in Fig. 3(b) is a microstructure constructed with the initial set of design parameters for the two fibers in the optimization scheme. The optimized SSRVE is obtained by solving the proposed optimization scheme, as shown in Fig. 3(c). For the optimization procedure, the population size of the genetic algorithm is set to 60, and the iterative calculation in the optimization scheme stops when the number of generations since the last improvement of the minimum value of the objective function out of the populations, termed stall generations in MATLAB, reaches 25. Any other parameters are set to default values in the global optimization toolbox in MATLAB.

The PSD of the target microstructure and the SSRVEs are also shown under each microstructure in Fig. 3. The origin of the PSD is located at the center of each cube. The PSD of the initial SSRVE is quite different from that of the target microstructure, while the PSD of the optimized SSRVE is similar to that of the target microstructure. The objective function converges to almost zero by the optimization, as shown in **Fig. 4**. Therefore, the proposed optimization scheme works well in this example.

4. Validation of SSRVE for SFCs

This section provides a construction result for an SSRVE for SFCs using a real target microstructure. The mechanical properties of the target microstructure and the SSRVE are thus computed by NMT, and the proposed method is validated by comparison between the mechanical behavior of the target microstructure and that of the SSRVE.

4. 1 Construction of SSRVE

The SSRVE was constructed using the real target microstructure shown in **Fig. 5**. The target microstructure (Fig. 5(a)) was obtained using X-ray CT scans of a SFC plate prepared in accordance with ISO 294-3. The X-ray CT scans were performed with a voxel size of 1.3 μm and CT images were reconstructed using the image reconstruction system developed by Uesugi et al.[23] The fiber volume fraction and the fiber diameter in the target microstructure were
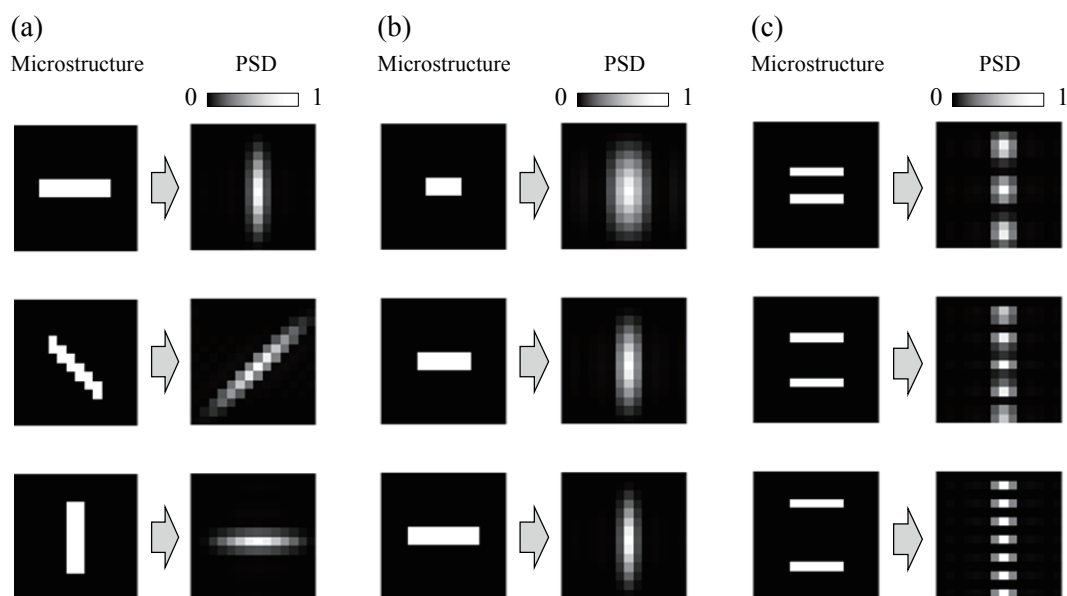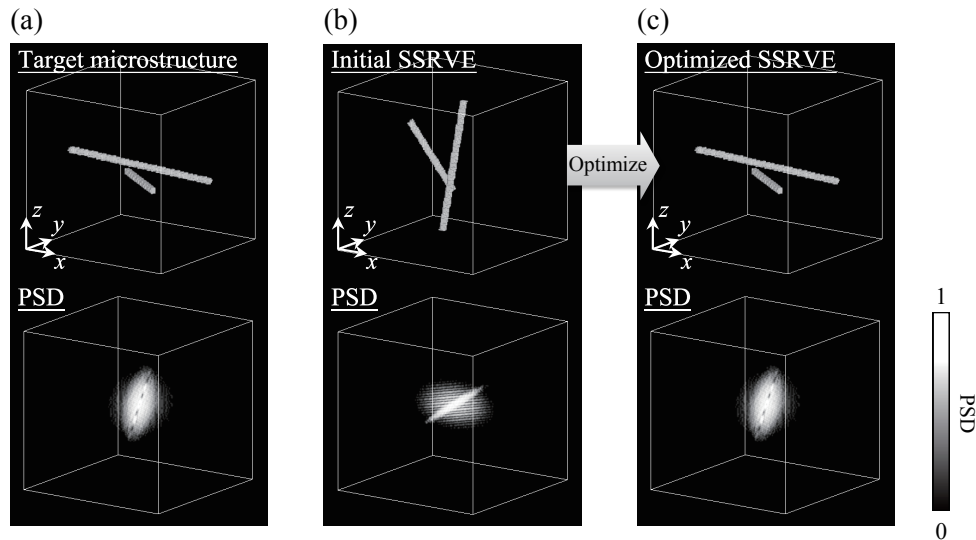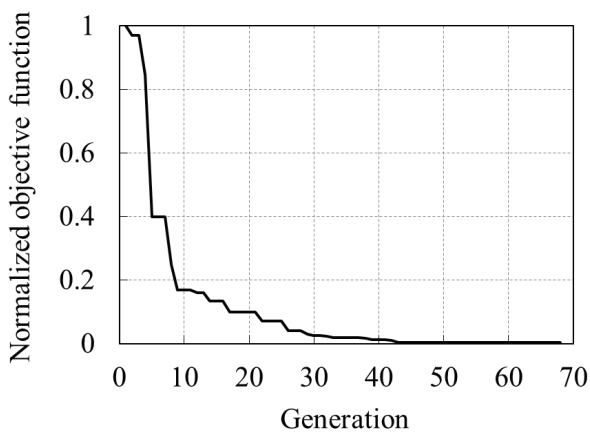

Fig. 2　Influence of fiber orientation (a), fiber length (b), and fiber interval (c) on PSD.

Fig. 3   Fiber distribution and PSD of target microstructure (a), initial SSRVE (b), and optimized SSRVE (c) for verification of optimization scheme.

Fig. 4   Convergence behavior in optimization scheme. The vertical axis represents the best objective function out of the populations normalized with respect to the first generation. The normalized objective function for the last generation is approximately 0.0394.

approximately 22% and 0.008 mm, respectively. The fiber length distribution in the target microstructure was measured, as shown in **Fig. 6**. The mean fiber length weighted by length was approximately 0.5 mm. Herein, the mechanical properties of the target microstructure are assumed to be strongly affected by the mean fiber length. Therefore, the fiber length in the SSRVE was set to 0.5 mm. The fiber diameter in the SSRVE was identical to that in the target

microstructure. The dimensions of the SSRVE and the number of fibers were set to $0.056 \times 0.225 \times 0.225$ mm^3 and 90, respectively, in such a way that the fiber volume fraction in the target microstructure was as similar as possible to that in the SSRVE. For the optimization procedure in this section, the population size was set to 200 and the optimization iteration was stopped when the stall generations reached 50. The SSRVE (Fig. 5(b)) is constructed by solving the optimization scheme and the PSD of the SSRVE is similar to that of the target microstructure, as shown in Fig. 5.

4. 2 Model Description for NMT

The mechanical properties of the target microstructure (Fig. 5(a)) and the optimized SSRVE (Fig. 5(b)) were evaluated using NMT in terms of stress-strain curves under uniaxial tensile loading. The finite element discretization of the target microstructure consists of 3423580 nodes and 19898465 tetrahedral elements, while the finite element model of the SSRVE consists of 38376 nodes and 214648 tetrahedral elements. These finite element models are constructed using the commercial 3D image analysis software Simpleware ScanIP.

A geometrically nonlinear, elastoplastic model in Abaqus/Standard is used for the constitutive model of fibers and a matrix. In this model, the Jaumann rate τ^{∇}, of the Kirchhoff stress τ, is defined as:

(a)　　　　　　　　　　　　(b)
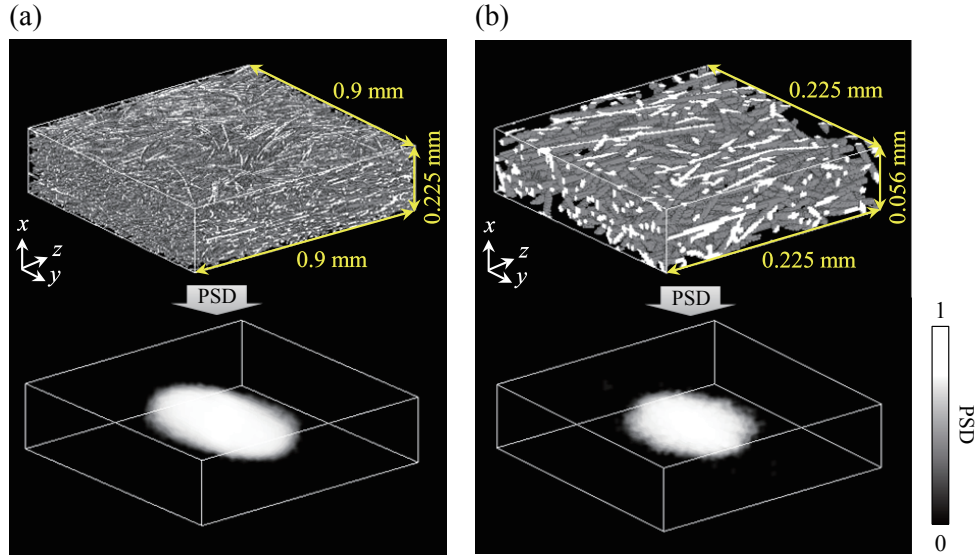
Fig. 5　Fiber distribution and PSD of real target microstructure (a) and optimized SSRVE (b) for SFCs.
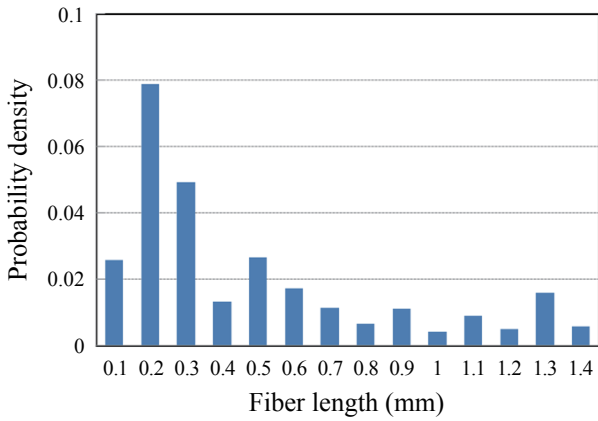
Fig. 6　Fiber length distribution weighted by length in real target macrostructure.

$$\boldsymbol{\tau}^{\nabla} = \dot{\boldsymbol{\tau}} - \boldsymbol{W}\boldsymbol{\tau} - \boldsymbol{\tau}\boldsymbol{W} = \mathbb{C} : \left(\boldsymbol{D} - \boldsymbol{D}^p \right), \tag{10}$$

where the superposed dot denotes the material time derivative, $\mathbb{C}$ is the tangent modulus tensor for $\boldsymbol{\tau}^{\nabla}$, and $\boldsymbol{D}$ and $\boldsymbol{W}$ are the symmetric and antisymmetric parts of the spatial velocity gradient, respectively. Herein, $\boldsymbol{D}$ is decomposed into the elastic part and the plastic part as:

$$\boldsymbol{D} = \boldsymbol{D}^e + \boldsymbol{D}^p. \tag{11}$$

Furthermore, $\boldsymbol{D}^p$ follows the associated flow rule:

$$\boldsymbol{D}^p = \gamma \frac{\partial f}{\partial \boldsymbol{\sigma}} = \gamma \frac{\boldsymbol{\sigma}}{\|\boldsymbol{\sigma}\|}, \tag{12}$$

with the plastic multiplier γ and the Cauchy stress $\boldsymbol{\sigma}$. f is the von Mises yield criterion:

$$\begin{aligned} f\left(\boldsymbol{\sigma}, \alpha\right) &= \|\boldsymbol{S}\| - \sqrt{\frac{2}{3}}\left(\sigma_{\mathrm{Y}} + K\alpha\right) \\ &= \sqrt{\boldsymbol{S} : \boldsymbol{S}} - \sqrt{\frac{2}{3}}\left(\sigma_{\mathrm{Y}} + K\alpha\right), \end{aligned} \tag{13}$$

with the equivalent plastic strain α, the yield stress σ_{Y} and the isotropic hardening coefficient K. Herein, $\boldsymbol{S}$ is the deviatoric component of $\boldsymbol{\sigma}$, which is defined as:

$$\boldsymbol{S} = \boldsymbol{\sigma} - \frac{\mathrm{tr}(\boldsymbol{\sigma})}{3}\boldsymbol{I}, \tag{14}$$

where $\mathrm{tr}(\boldsymbol{\sigma})$ is the trace of $\boldsymbol{\sigma}$ and $\boldsymbol{I}$ is the 2nd-order identity tensor. α in Eq. (13) follows the evolution equation formulated as:

$$\dot{\alpha} = \sqrt{\frac{2}{3}}\|\boldsymbol{D}^p\| = \gamma\sqrt{\frac{2}{3}}. \tag{15}$$

The material parameters of fibers and matrix are summarized in **Table 1**. In addition, the isotropic hardening coefficient of the matrix was set by inputting the polyline curve shown in **Fig. 7** as the relationship

between the true stress and the equivalent plastic strain using *PLASTIC in Abaqus/Standard. These parameters are based on the material properties of the T300 carbon fiber[24] and polyamide 6.[25]

Tensile analyses of the target microstructure and the SSRVE were performed under the linear displacement boundary conditions and periodic boundary conditions, respectively, using an Intel Xeon processor E5-2667 v2 and NVIDIA Tesla K20X GPUs. The linear displacement boundary conditions and periodic boundary conditions were implemented by multi-point constraint equations in Abaqus/Standard, cf. the literature.[7]

4. 3 NMT for SFCs

Stress-strain curves obtained by NMT are shown in **Fig. 8**. The macroscopic stresses and strains are equal to the volume average of the nominal stress and strain at the microscopic scale, respectively. They were computed from the reaction forces and displacements of the control nodes.[7] The stress and strain components in the loading direction are shown. The macroscopic properties of the target microstructure and the SSRVE

are depicted with lines and circles, respectively. In addition, the black, red, and blue data present the tensile properties in the x-, y- and z-directions, respectively. Figure 8 shows that the mechanical response of the SSRVE is in good agreement with that of the target microstructure. Finally, the computational costs of NMT and the optimization scheme are shown in **Table 2**. The numerical material tests using the target microstructure took approximately 2855 min on average, whereas the NMTs using the SSRVE took approximately 136 min on average. Therefore, NMT using the SSRVE realized a 95 percent reduction in the computational costs of NMT in this example. Furthermore, the computational cost of the SSRVE, which is the total cost of the NMTs and the optimization scheme, was 29 percent of the total computational cost of the NMTs using the target microstructure. Note that the optimization scheme for the construction of the SSRVE is only a one-time effort.

One of the main advantage of SSRVEs is their periodicity. The SSRVEs can include fibers that cross the boundaries of the SSRVEs. In contrast, target microstructures cannot include the fibers that cross their boundaries, because they are not periodic. Therefore, the fibers that cross the boundaries of the target microstructures should be cut, as shown in Fig. 5(a). This cutting causes a change of the fiber length distribution. Therefore, the size of the target microstructure should be sufficiently large to extinguish the influence of this cutting on the

Table 1   Material parameters of fibers and matrix for NMT.

	Fiber	Matrix
Young's modulus	231 GPa	2.6 GPa
Poisson's ratio	0.2	0.35
Yield stress σ_Y	-	78 MPa
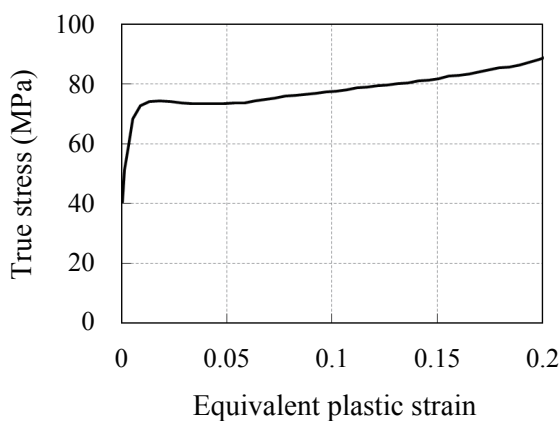
Fig. 7   Hardening behavior of polyamide 6.
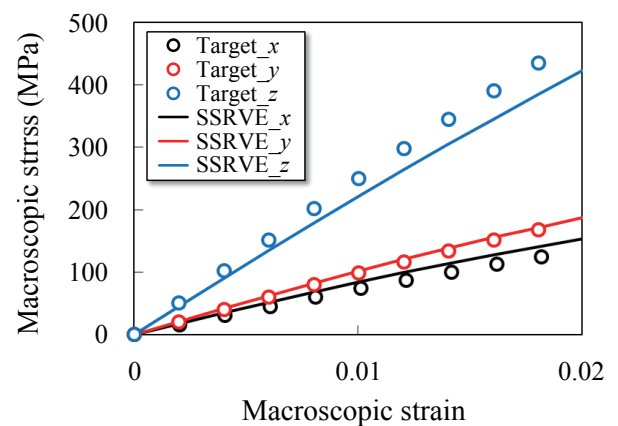
Fig. 8   Macroscopic tensile properties in x-direction, y-direction, and z-direction. Circles and solid lines indicate mechanical properties of target microstructure and SSRVE, respectively.

Table 2 Comparison of CPU time T_{target} and T_{SSRVE} in NMT with target microstructure and SSRVE with high volume fraction of fiber.

	Tensile analyses			Optimization	Summation
Direction	x	y	z	-	-
T_{target} (min)	2926	2505	3135	-	8566
T_{SSRVE} (min)	135	141	132	2088	2496
T_{SSRVE} / T_{target}	0.0461	0.0563	0.0421	-	0.291

macroscopic properties obtained by NMT. As a result, the size of the SSRVEs can be smaller than that of the target microstructure, and the computational cost of the SSRVEs will be lower than that of the target microstructure.

5. Conclusions

A computational method for the construction of SSRVEs for SFCs was proposed to efficiently evaluate the mechanical properties of SFCs. It was assumed that the mechanical response of SFCs is strongly affected by the PSD of their microstructures. Based on this assumption, an SSRVE was constructed by solving an optimization problem that minimizes the difference between the PSD of a real target microstructure and that of a SSRVE. The proposed method was validated through a comparison of the mechanical response computed by NMT with the real target microstructure and that obtained by NMT with the SSRVE. The numerical results demonstrate that the mechanical properties of the SSRVE are consistent with those of the real target microstructure, and a 95 percent reduction in the computational costs of the NMT for SFCs was realized.

References

(1) Krause, W., Henning, F., Tröster, S., Geiger, O. and Eyerer, P., "LFT-D: A Process Technology for Large Scale Production of Fiber Reinforced Thermoplastic Components", *Journal of Thermoplastic Composite Materials*, Vol. 16, No. 4 (2003), pp. 289-302.

(2) Eshelby, J. D., "The Determination of the Elastic Field of an Ellipsoidal Inclusion, and Related Problems", *Proceedings of the Royal Society of London, Series A: Mathematical, Physical and Engineering Sciences*, Vol. 241, No. 1226 (1957), pp. 376-396.

(3) Mori, T. and Tanaka, K., "Average Stress in Matrix and Average Elastic Energy of Materials with Misfitting Inclusions", *Acta Metallurgica*, Vol. 21, No. 5 (1973), pp. 571-574.

(4) Hill, R., "A Self-consistent Mechanics of Composite Materials", *Journal of the Mechanics and Physics of Solids*, Vol. 13, No. 4 (1965), pp. 213-222.

(5) Nguyen, B. N., Bapanapalli, S. K., Kunc, V., Phelps, J. H. and Tucker III, C. L., "Prediction of the Elastic–plastic Stress/Strain Response for Injection-molded Long-fiber Thermoplastics", *Journal of Composite Materials*, Vol. 43, No. 3 (2009), pp. 217-246.

(6) Advani, S. G. and Tucker III, C. L., "The Use of Tensors to Describe and Predict Fiber Orientation in Short Fiber Composites", *Journal of Rheology*, Vol. 31, No. 8 (1987), pp. 751-784.

(7) Terada, K., Kato, J., Hirayama, N., Inugai, T. and Yamamoto, K., "A Method of Two-scale Analysis with Micro-macro Decoupling Scheme: Application to Hyperelastic Composite Materials", *Computational Mechanics*, Vol. 52, No. 5 (2013), pp. 1199-1219.

(8) Terada, K., Hirayama, N., Yamamoto, K., Kato, J., Kyoya, T., Matsubara, S., Arakawa, Y., Ueno, Y. and Miyanaga, N., "Applicability of Micro–macro Decoupling Scheme to Two-scale Analysis of Fiber-reinforced Plastics", *Advanced Composite Materials*, Vol. 23, No. 5-6 (2014), pp. 421-450.

(9) Terada, K., Hirayama, N., Yamamoto, K., Muramatsu, M., Matsubara, S. and Nishi, S., "Numerical Plate Testing for Linear Two-scale Analyses of Composite Plates with In-plane Periodicity", *International Journal for Numerical Methods in Engineering*, Vol. 105, No. 2 (2016), pp. 111-137.

(10) Fish, J. and Shek, K., "Finite Deformation Plasticity for Composite Structures: Computational Models and Adaptive Strategies", *Computer Methods in Applied Mechanics and Engineering*, Vol. 172, No. 1-4 (1999), pp. 145-174.

(11) Miehe, C., Schotte, J. and Schröder, J., "Computational Micro–macro Transitions and Overall Moduli in the Analysis of Polycrystals at Large Strains", *Computational Materials Science*, Vol. 16, No. 1-4 (1999), pp. 372-382.

(12) Feyel, F. and Chaboche, J.-L., "FE^2 Multiscale Approach for Modelling the Elastoviscoplastic Behaviour of Long Fibre SiC/Ti Composite Materials", *Computer Methods in Applied Mechanics and Engineering*, Vol. 183, No. 3-4 (2000), pp. 309-330.

(13) Terada, K. and Kikuchi, N., "A Class of General Algorithms for Multi-scale Analyses of Heterogeneous Media", *Computer Methods in Applied Mechanics and Engineering*, Vol. 190, No. 40-41 (2001), pp. 5427-5464.

(14) Geers, M. G. D., Kouznetsova, V. G. and Brekelmans, W. A. M., "Multiscale First-order and Second-order Computational Homogenization of Microstructures towards Continua", *International Journal for Multiscale Computational Engineering*, Vol. 1, No. 4 (2003), pp. 371-386.

(15) Fliegener, S., Luke, M. and Gumbsch, P., "3D Microstructure Modeling of Long Fiber Reinforced Thermoplastics", *Composites Science and Technology*, Vol. 104 (2014), pp. 136-145.

(16) Balzani, D., Brands, D., Schröder, J. and Carstensen, C., "Sensitivity Analysis of Statistical Measures for the Reconstruction of Microstructures Based on the Minimization of Generalized Least-square Functionals", *Technische Mechanik*, Vol. 30, No. 4 (2010), pp. 297-315.

(17) Ambrozinski, M., Bzowski, K., Rauch, L. and Pietrzyk, M., "Application of Statistically Similar Representative Volume Element in Numerical Simulations of Crash Box Stamping", *Archives of Civil and Mechanical Engineering*, Vol. 12, No. 2 (2012), pp. 126-132.

(18) Balzani, D., Scheunemann, L., Brands, D. and Schröder, J., "Construction of Two- and Three-dimensional Statistically Similar RVEs for Coupled Micro-macro Simulations", *Computational Mechanics*, Vol. 54, No. 5 (2014), pp. 1269-1284.

(19) Rauch, L., Kuziak, R. and Pietrzyk, M., "From High Accuracy to High Efficiency in Simulations of Processing of Dual-phase Steels", *Metallurgical and Materials Transactions B*, Vol. 45, No. 2 (2014), pp. 497-506.

(20) Brands, D., Balzani, D., Scheunemann, L., Schröder, J., Richter, H. and Raabe, D., "Computational Modeling of Dual-phase Steels Based on Representative Three-dimensional Microstructures Obtained from EBSD Data", *Archive of Applied Mechanics*, Vol. 86, No. 3 (2016), pp. 575-598.

(21) Schröder, J., Balzani, D. and Brands, D., "Approximation of Random Microstructures by Periodic Statistically Similar Representative Volume Elements Based on Lineal-path Functions", *Archive of Applied Mechanics*, Vol. 81, No. 7 (2011), pp. 975-997.

(22) Scheunemann, L., Balzani, D., Brands, D. and Schröder, J., "Design of 3D Statistically Similar Representative Volume Elements Based on Minkowski Functionals", *Mechanics of Materials*, Vol. 90 (2015), pp. 185-201.

(23) Uesugi, K., Hoshino, M., Takeuchi, A., Suzuki, Y., Yagi, N. and Nakano, T., "Development of Fast (Sub-minute) Micro-tomography", *AIP Conference Proceedings*, Vol. 1266, No. 1 (2010), pp. 47-50.

(24) Kaddour, A. S. and Hinton, M. J., "Input Data for Test Cases Used in Benchmarking Triaxial Failure Theories of Composites", *Journal of Composite Materials*, Vol. 46, No. 19-20 (2012), pp. 2295-2312.

(25) Huang, J., Schmauder, S., Weber, U. and Geier, S., "Micromechanical Modelling of the Elastoplastic Behaviour of Nanodispersed Elastomer Particle-modified PA 6", *Computational Materials Science*, Vol. 52, No. 1 (2012), pp. 107-111.

Takashi Sasagawa
  Research Field:
    - Material Modeling for Finite Element
      Analysis
  Academic Societies:
    - The Japan Society of Mechanical Engineers
    - The Japan Society for Computational Engineering
      and Science
  Award:
    - JSCES The Outstanding Paper Award, The Japan
      Society for Computational Engineering and Science,
      2018

Masato Tanaka
  Research Field:
    - Nonlinear Material Modeling
  Academic Degree: Dr.Eng.
  Academic Societies:
    - The Japan Society of Mechanical Engineers
    - The Japan Society for Computational Engineering
      and Science
  Awards:
    - JSME Young Engineers Award, The Japan Society of
      Mechanical Engineers, 2012
    - JSCES The Outstanding Paper Award, The Japan
      Society for Computational Engineering and Science,
      2018

Ryuji Omote
  Research Fields:
    - Numerical Modeling
    - Structural Mechanics
  Academic Degree: Dr.Eng.
  Academic Societies:
    - The Japan Society of Mechanical Engineers
    - The American Society of Mechanical Engineers
    - The Japan Society for Computational Engineering
      and Science
  Award:
    - JSCES The Outstanding Paper Award, The Japan
      Society for Computational Engineering and Science,
      2018